Isomer-specific, Cryogenic Ion Vibrational Spectroscopy Investigation of D_2- and N_2- Tagged, Protonated Formic Acid Complexes Using Two Color, IR-IR Photobleaching

Erica L. Bocanegra,[a] Abhijit Rana,[a] Anne B. McCoy,[b]* and Mark A. Johnson[a]*

[a]Sterling Chemistry Laboratory, Department of Chemistry Yale University, New Haven, CT USA

[b]Department of Chemistry, University of Washington, Seattle, WA USA

*Corresponding Authors, Email: mark.johnson@yale.edu, abmcoy@uw.edu

Abstract

Here we analyze cryogenic ion vibrational spectra of tagged protonated formic acid (PFA) with electronic structure and anharmonic vibrational calculations to establish the isomers generated by electrospray ionization (ESI) followed by buffer gas cooling to ~25 K. Two isomers are identified (the *trans* form (E,Z) and the *cis* form (E,E)) and generated in comparable abundance despite the fact that the calculated E,E structure lies 6.40 kJ mol^{-1} above the E,Z form. A large (~60 kJ mol^{-1}) barrier separates them such that the E,E form can be kinetically trapped upon cooling in the ion trap. The anticooperativity between the H-bonds of the OH groups is explored by measuring the shift in the D_2-bound OH fundamental when a second D_2 is attached. Both isomers are observed in the N_2-tagged counterparts, displaying the expected red-shifted OH bands. These results indicate that ESI generates both isomers and both must be considered when analyzing cluster spectra based on the PFA core ion.

TOC Graphic

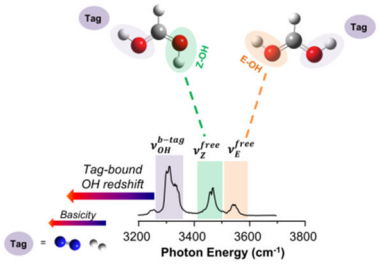

While neutral formic acid (FA) is known to catalyze isomerization reactions in the gas phase,[1] its protonated form (hereafter PFA) has recently been implicated[2] as the key species responsible for the acceleration of reactions in the microdroplet regime.[3,4,5,6] PFA and related protonated species are thought to be present due to the highly acidic conditions at the air-water interface of the microdroplet. (pH~ -1 to 3 with droplet diameters < 1 micron).[7,8] The three possible PFA isomers that occur by attachment of a proton to the carbonyl group of the neutral acid are indicated in Figure 1, which feature two OH groups that vary according to their orientations (denoted E and Z) relative to the CH bond axis.[9,10] We note that another isomer has been identified[11] in which both protons bind to one of the oxygen atoms. That structure corresponds to the entrance channel of the dehydration reaction of PFA to yield HCO^+, which is a particularly abundant molecular ion in interstellar space.[12,13,14] An earlier study[15] of the D_2-tagged PFA-$(H_2O)_{n=0-10}$ cluster ions focused on the speciation of the "excess proton" upon microhydration. Analysis of the vibrational band patterns obtained using cryogenic ion spectroscopy[16] with path integral theoretical methods[17,18] indicated that the proton migrates to the water network by n=3 or 4. That study only considered the lowest energy E,Z scaffold, however, and here we revisit the PFA isomers generated by electrospray ionization and cooled in a cryogenic ion trap using isomer-selective, two-color, IR-IR photobleaching of D_2- and N_2-tagged PFA. This study is an extension of recent work[19] that focused on the structures at play in the less acidic protonated 4-aminobenzoic (4-ABA) system (proton affinities (PA): PA_{4-ABA} = 865 kJ mol^{-1}, PA_{FA} = 742 kJ mol^{-1}), where in that case, only the E,Z isomer was formed after cooling the nascent ions generated by ESI.

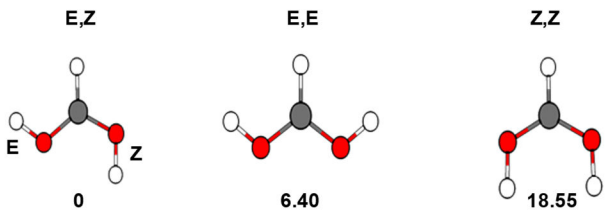

Figure 1. Geometry optimized structures of protonated formic acid (PFA, $HCO_2H_2^+$) rotamers with E and Z configurations relative to the CH bond axis, obtained at the MP2/aug-cc-pVTZ level of theory. Anharmonic ZPE corrected relative energies (kJ mol^{-1}), calculated at the same level of theory, are displayed below the structures.

Figure 2a presents the experimental IRPD spectrum of PFA-D_2 in the 2800 cm^{-1} - 3800 cm^{-1} range. The lowest energy feature near 2900 cm^{-1} is due to the D_2 fundamental (labeled 6, ν_{D_2}), which is typically activated upon attachment to OH groups.[27] Five distinct bands appear in the region that is associated with the OH stretching fundamental, numbered 1 through 5 in Figure 2a. The nominal frequencies of the free OH stretches for the E (cis) and Z (trans) forms of the neutral formic acid molecule[28] (denoted ν_E^{FA} and ν_Z^{FA}) are indicated by the dashed lines at the top of Figure 2.

To identify the number of isomers present in D_2-tagged PFA and isolate their spectral patterns, we carried out an isomer-selective photobleaching study with the results presented in Figure 2b-2d. Each upward going trace was obtained by bleaching the ion packet with the modulated pump laser located at the transitions indicated by color-coded arrows in Figure 2a. Three distinct patterns (denoted I, II, and III) are recovered, albeit with some overlapping bands (e.g. peaks 3 and 4).

A useful clue to the assignment of structures responsible for the three band patterns is the separation (75 cm^{-1}) between the two higher energy bands (1 and 2), at 3540 cm^{-1} and 3465 cm^{-1}, respectively. This is close to the splitting (68 cm^{-1}) between the E and Z OH fundamentals in FA (ν_E^{FA} and ν_Z^{FA} at the top of Fig. 2) with the centroid of the two PFA-D_2 bands lying 83 cm^{-1} below that of the pair in FA. This suggests assignment of bands 1 and 2 to PFA structures with non-bonded OH groups in the E and Z positions, respectively, while the lower energy bands (3-5) are associated with the D_2-bound OH analogues. With that scheme, the I and II spectra both display features near band 1, as emphasized by the blue dashed vertical line in Figure 2, indicating the

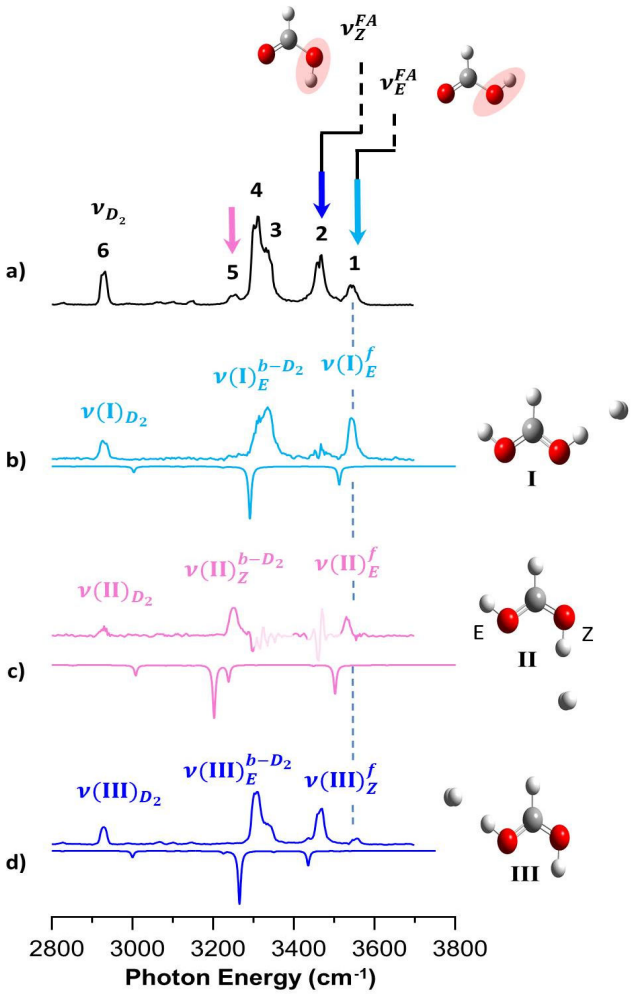

Figure 2. a) D_2-tagged vibrational spectrum of PFA with OH stretching bands labeled 1-5. b)-d) Colored upward traces are isomer-specific spectra obtained through modulation of isomer populations by bleaching at the frequencies indicated by colored arrows in a) (peak 1 bleach in cyan, peak 2 bleach in dark blue, peak 5 bleach in pink); b) isomer I (E,E), c) isomer II (E,Z configuration, D_2 tag on Z), and d) isomer III (E,Z configuration with D_2 tag on E). The splitting between the E and Z OHs in neutral FA is indicated above trace a) with the structures shown in the inset, and is compared to the splitting of the free OHs in PFA-D_2 via black lines. See text for explanation of band labels. Calculated local minimum energy structures are displayed at the right, with corresponding anharmonic spectra shown inverted under the observed isomer-selective spectra. Shaded regions of the modulated spectrum in c) indicate noise arising from incomplete subtraction of intense bands from other isomers.

presence of a free E OH group. As such, the two isomers responsible for the I and II spectra differ according to whether D_2 attaches to the companion E or Z OH groups, while isomer III yields band 2 which indicates that is has a free Z OH. In the case where the D_2 binding energies are similar in both OH positions, this would lead to red-shifted OH bands displaced by a similar amount from the non-bonded E and Z OH frequencies. The lower energy features in the spectra of isomers I and II, (bands 3 and 5, with band 3 clearly overlapping with another band that is associated with isomer III) are separated by 87 cm^{-1}, which is close to that observed (75 cm^{-1}) between peaks 1 and 2. This suggests the assignment scheme displayed in the structures at the right of Figure 2c and 2d, which are indeed recovered as minimum energy structures. Hereafter, band assignments are indicated by the notation $\nu(k)_{E\ or\ Z}^{b-D_2}$ and $\nu(k)_{E\ or\ Z}^{f}$, (k=I, II or III) that indicate whether the OH (E or Z) groups are bound (b) or free (f) and associated with isomer pattern, k. The lowest energy OH feature in the III pattern (Fig. 2d) is the carrier of band 4, which lies very close to that assigned to $\nu(\mathrm{I})_{E}^{b-D_2}$. This suggests that band 4 similarly arises a D_2-bound E OH, $\nu(\mathrm{III})_{E}^{b-D_2}$. Since band 2 was already assigned to the Z OH, we conclude that the isomer III structure is based on PFA in the E,Z configuration with the minimum energy structure displayed to the right of Figure 2d.

The calculated anharmonic spectra for the three structures are displayed inverted in Figure 2b, 2c and 2d. The predicted OH stretching transitions are all systematically about 30 cm^{-1} below those observed while the D_2 frequencies are all roughly 75 cm^{-1} higher than those that are observed. In all cases, though, the overall relative patterns are well recovered, supporting the structure assignments. The calculated anharmonic frequencies are compared with the experimental values in Table S1 for both FA and PFA-D_2 ions.

The fact that all features in the spectra can be assigned to the E,E and E,Z conformers is consistent with the theoretical predication that the missing Z,Z structure lies much higher (~18 kJ mol^{-1}) in energy than the E,Z conformer (see Figure 1). Isomers II and III differ according to whether the D_2 tag attaches to the E or Z OH groups, and the much larger relative population of isomer III is consistent with the anharmonic VPT2 calculations that place isomer II 0.6 kJ mol^{-1} above isomer III (when anharmonic zero-point energy is considered (see Table S2)). It is expected that the relative populations of these isomers will reflect this energy difference because they are readily interconverted by bimolecular, low energy collisions in the trap that can change the docking location of the tag[29]:

$$\mathrm{E,Z\text{-}(D_2)^{(II)} + D_2 \rightarrow [E,Z\text{-}(D_2)_2]^* \rightarrow E,Z\text{-}(D_2)^{(III)} + D_2} \qquad [1]$$

Isomer I, on the other hand, is based on a different PFA scaffold (E,E), which is calculated to lie 6.40 kJ mol^{-1} above the E,Z form and yet is generated with a similar population to that of isomer III, as indicated by the relative intensities of the transitions. Note that only one D_2-tagged species is generated upon tagging isomer I since the OH groups are symmetrical. The generation of isomer I in comparable abundance to that of isomer III is surprising, and in fact this isomer was not considered in the earlier report[15] because it lies so far energetically above the ground state E,Z form. This observation can be rationalized, however, by the fact that the E,Z and E,E structures are separated by a large (~60 kJ mol^{-1} at DFT:B3LYP/ 6-311+G(d,p) level of theory) barrier, and thus their relative populations likely reflect kinetic trapping upon initial cooling in the trap.[22,23]

For completeness, we recorded the isomer-selective spectra of the isomer I and III species in the fingerprint region with the results presented in Figure S1. Both spectra are dominated by a sharp transition traced to the asymmetric CO_2 stretch[30] near 1680 cm^{-1} that is only slightly dependent ($\pm$10 cm^{-1}) on the isomer structure (experimental and calculated frequencies reported in Table S3).

To explore the degree of cooperativity between the OH groups, we followed the evolution of the bands from both E,Z and E,E scaffolds upon the addition of a second D_2 tag molecule. Application of this strategy to the E,Z form of PFA is displayed in Figure 3b, which is compared with the two singly tagged species in Figure 3a (bound Z) and 3c (bound E). The E,Z-$(D_2)_2$ spectrum was isolated from that of the E,E-$(D_2)_2$ isomer by IR-IR photobleaching with the results displayed in Figure S2. The E,Z-$(D_2)_2$ is dominated by a strong doublet with a splitting (72 cm^{-1}) that primarily reflects the intrinsic difference (75 cm^{-1}) between the frequencies of the free Z and E OH groups. The black horizontal brackets illustrate the displacements of the free Z and E OH oscillators upon forming the doubly tagged cluster. We note that each of the bound OH bands in the doubly tagged species is displaced above their singly tagged analogues by ~25 cm^{-1}, which reflects the degree of anticooperativity (AC)

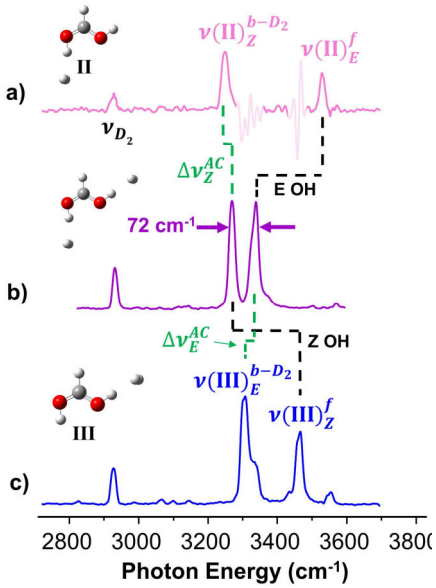

Figure 3. a) and c) D_2-tagged vibrational spectra of isomer II and isomer III of PFA-D_2, respectively. b) Vibrational spectrum of the E,Z isomer of PFA-$(D_2)_2$. Redshift of the free E and Z OH bands on the E,Z scaffold upon addition of a second D_2 tag indicated by dashed black lines. Green dashed lines indicate the anticooperativity (AC) of the H-bonds to E and Z OHs ($\Delta\nu_E^{AC}$ or $\Delta\nu_Z^{AC}$). The splitting between the E and Z OHs for PFA-$(D_2)_2$ is indicated by the inward facing arrows in trace b. Shaded regions of the modulated spectrum in b) indicate noise arising from incomplete subtraction of intense bands from other isomers.

between the two distant OH groups (this effect is denoted by $\Delta\nu_Z^{AC}$ and $\Delta\nu_E^{AC}$ in Figure 3). This occurs when attachment of the second D_2 acts to slightly weaken the original hydrogen bond to the first tag, so both D_2-bound OHs are blueshifted in the double D_2-tagged ternary complex compared to the bound OHs in the singly tagged complex. We also explored the evolution of the OH bands upon adding a second tag to the E,E isomer with the results presented in Figure S2 (frequencies reported in Table S4), which is, dominated by a single OH feature in this symmetrical complex. This is captured in the calculated anharmonic spectrum (see Figure S3), where intensity in the out-of-phase OH stretching vibration is an order of magnitude larger than the in-phase stretch. In contrast, on the basis of VPT2 calculations, the two OH stretching vibrations in isolated PFA are expected to have comparable intensities. The enhancement of the intensity of the out-of-phase stretching motion in the ternary complex reflects the fact that this vibration drives the system toward a complex between HD_2^+ and a neutral formic acid molecule that retains the second D_2. This results in a large change in the charge distribution depending on the phase of the vibration, and is analogous to the large intensity of the out-of-phase OH stretching vibration when a hydronium ion is complexed with two water molecules.[24]

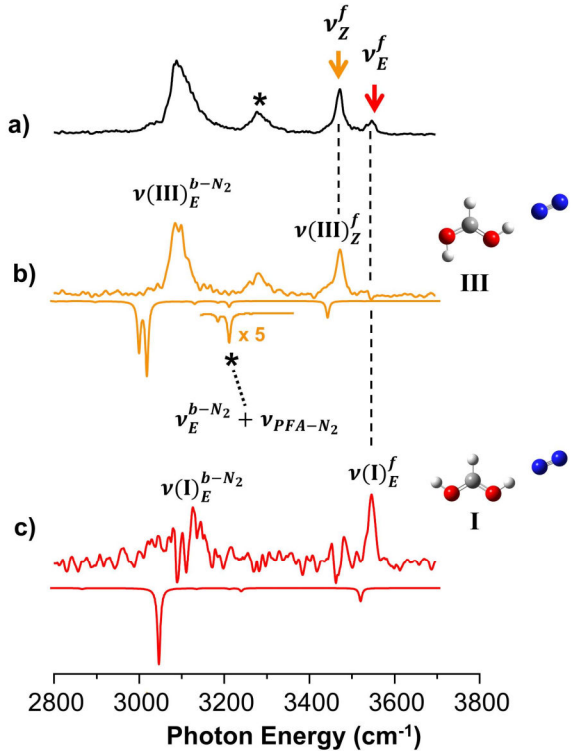

Figure 4. a) Single laser vibrational spectrum of N_2-tagged PFA, b) spectrum modulated by bleaching at the free Z OH (ν_Z^f) transition (orange arrow in a)), and c) spectrum modulated by bleaching at the free E OH (ν_E^f) transition (red arrow in a)).Calculated minimum energy structures are displayed at the right, with corresponding anharmonic spectra shown inverted under the observed isomer-selective spectra. The intensity of the peak labeled * in the calculated spectrum of trace b) is amplified by 5x to ease visualization.

We next turn to the degree of deformation of the PFA scaffold upon attachment of a more strongly bound tag, N_2. The IRPD spectrum of the PFA-N_2 cluster is displayed in Fig. 4a. The two bands highest in energy appear very close to those assigned to the free E and Z OH groups in the D_2-tagged spectra, indicating the formation of at least two isomers. A third strong band near 3100 cm^{-1} appears about 230 cm^{-1} below the D_2-bound OH ($\nu_E^{b-D_2}$) bands with a weaker

interloper (labeled * in Figure 4a).

Isomer-selective spectra are displayed in Fig. 4b and 4c that correspond to photobleaching at the energies of the free E and Z bands (downward arrows in Fig. 4a.). The observed spectrum is recovered by two distinct patterns, indicating that two isomers are present as expected, with free OH transitions assigned to the E and Z orientations. Note that the (*) band in the non-selective spectrum (Figure 4a) is associated with the isomer that is responsible for the free Z OH band and likely arises from anharmonic couplings between the OH oscillator that is bound to the N_2, and the intermolecular N_2-PFA vibration (which has a harmonic frequency of 190 cm^{-1}). The empirical assignments of structural motifs are supported by the calculated minimum energy structures indicated at the right of Figure 4. The two isomers are variations of the I and III structures observed in the D_2-tagged PFA spectra with similar relative populations as evidenced by the intensities of the $\nu(\mathrm{I})_Z^{b-N_2}$ and $\nu(\mathrm{III})_E^{b-N_2}$ transitions. This behavior shows once again that the higher energy E,E isomer is present in the ion ensemble cooled in the trap. Note that we could not find evidence for the N_2-tagged variant of isomer II in the PFA-D_2 system, which was least abundant of the three. The fact that it is missing in the N_2-tagged ensemble is readily explained, however, by the bimolecular collision interconversion process (Eq. [1]) that is operative between the II-III isomers. Because of the larger energy separation between II and III (2.15 kJ mol^{-1}, see Table S2) in the more strongly bound N_2 case, the equilibrium population of II in an ensemble equilibrated at 20 K is expected to be dramatically suppressed (<< 1%).

With the isomer structures in hand, it is useful to consider the red shift in the context of general propensities reported earlier[31] in which the frequency of the proton shared between two bases is correlated with the difference in their proton affinities (PA) (PA_{D_2} = 410 kJ mol^{-1}, PA_{N_2} = 494 kJ mol^{-1}). Note that the large red-shift of the N_2-bound OH ($\nu_{OH}^{b-N_2}$) occurs while the spectator, non-bonded E and Z OH groups ($\nu(I)_E^f$ and $\nu(III)_Z^f$) are largely unaffected. This indicates that when non-bonded, the two OH groups in the E,Z configuration are essentially uncoupled. We also obtained the spectrum of the PFA-$(N_2)_2$ cluster with the result displayed in Figure S4. The doubly N_2-tagged system exhibits very similar behavior to that displayed by the PFA-$(D_2)_2$ cluster discussed above, consisting of a strong doublet traced to the bound E and Z OH groups, with the E OH higher in energy (all frequencies reported in Table S5).

Isomer-selective, cryogenic ion vibrational predissociation spectra of the D_2-tagged protonated formic acid cation reveal the formation of two core structures after cooling the ions generated by electrospray ionization to about 20 K in a Paul ion trap. The isomers correspond to the species with two OH groups such that one occurs with both OH groups oriented toward the CH bond (cis, E,E) while in the other, one is toward (E) and the other away (Z) from the CH (trans, E,Z). Both are generated in

comparable abundance despite the fact that the E,E isomer is calculated to lie 6.40 kJ mol^{-1} above the E,Z global minimum structure. Both PFA isomers are also observed in spectra of the N_2-tagged ion. This behavior is traced to the large barrier separating the isomers such that the higher energy isomer can be kinetically trapped upon buffer gas cooling. Establishing the species at play upon ESI generation of PFA thus clarifies the structures that contribute to reaction mechanisms invoked to rationalize the acceleration of reactions in the microdroplet regime.

METHODS

Experimental protocols

D_2 and N_2 predissociation spectra were recorded on the Yale triple focusing photofragmentation time-of-flight (TOF) mass spectrometer that has been described previously.[20,21] Pure formic acid was purchased from Sigma Aldrich with no further purification. Ionic species were generated via electrospray ionization (ESI) of a 10% aqueous formic acid solution in a humidity-controlled chamber. ESI ions were transferred through a series of differential pumping stages via radio frequency ion guides to a temperature controlled, 3D (Paul) ion trap operated from 5 K – 40 K. A buffer gas pulse containing He doped with a tagging gas (D_2 or N_2, 20%) was introduced to the 20 K trap with a duration of about 20 ms. Collisions with the He gas thermalize the ions to the temperature of the trap on a ms timescale[22,23] and the inert tagging gas condenses onto the ions during the cooling process. The tagged ions were then ejected from the Paul trap into the TOF photofragmentation mass spectrometer after being stored in the ion trap for ~90 ms.

Routine vibrational spectra were obtained over the 1000 cm^{-1} – 4000 cm^{-1} range by excitation with IR radiation from a LaserVision OPO/OPA (5 ns, 2-20 mJ/pulse) at a transient focus of the TOF. Absorption of a single resonant photon results in the loss of the weakly bound tags so that the infrared photodissociation (IRPD) spectra are obtained in a linear action mode. Isomer-specific vibrational spectra were obtained using a two color IR-IR photobleaching scheme.[24] In that method, a second 5 ns pulsewidth "bleach" laser intercepts the TOF ion packet at another transient TOF focus located before the scanned laser that generates the IRPD spectrum. The bleach laser is fixed at a transition frequency corresponding to a particular isomer and pulsed on at every other cycle of the 10 Hz experiment. The isomer-specific spectrum is then recovered by recording the "bleach on" - "bleach off" modulated photofragment signal from the scanned laser.

Theoretical calculations

All electronic structure calculations were performed using the Gaussian 16 program package[25] at the MP2/aug-cc-pVTZ level of theory/basis set. The coordinates of the optimized geometries are

provided in the Supplementary Materials. Anharmonic frequencies and intensities were obtained using the implementation of vibrational perturbation theory (VPT2) that is incorporated in the Gaussian program package. To facilitate comparisons with the measured spectra, where the ion signal is divided by the laser power, the calculated intensities also need to be divided by the energy of the transition as explained in detail earlier.[26]

Acknowledgements

The authors thank the Air Force Office of Research under the MURI grant 62742085-204669 (MAJ) and the Department of Energy under collaborative grants DE-SC0021012 (MAJ) and DE-SC0021081 (ABM). The AFOSR MURI grant supports our work on the properties of superacids at the surface of microdroplets, while the DOE grant supports work focused on the speciation of excess protons in aqueous media. The AFOSR award FA9550-18-1-0213 supported the original construction of the cryogenic ion vibrational spectroscopy instrument used in this study. ELB was supported by the Biophysical Training grant no. 5T32GM149438-02.

Supporting information available: Additional experimental and computational spectra and optimized geometries.

References

1. Vansco, M. F.; Caravan, R. L.; Pandit, S.; Zuraski, K.; Winiberg, F. A. F.; Au, K.; Bhagde, T.; Trongsiriwat, N.; Walsh, P. J.; Osborn, D. L.; Percival, C. J.; Klippenstein, S. J.; Taatjes, C. A.; Lester, M. I. Formic acid catalyzed isomerization and adduct formation of an isoprene-derived Criegee intermediate: experiment and theory. *Physical Chemistry Chemical Physics* **2020,** *22* (46), 26796-26805.
2. Basuri, P.; Gonzalez, L. E.; Morato, N. M.; Pradeep, T.; Cooks, R. G. Accelerated microdroplet synthesis of benzimidazoles by nucleophilic addition to protonated carboxylic acids. *Chemical Science* **2020,** *11* (47), 12686-12694.
3. Girod, M.; Moyano, E.; Campbell, D. I.; Cooks, R. G. Accelerated bimolecular reactions in microdroplets studied by desorption electrospray ionization mass spectrometry. *Chemical Science* **2011,** *2* (3), 501-510.
4. Bain, R. M.; Pulliam, C. J.; Ayrton, S. T.; Bain, K.; Cooks, R. G. Accelerated hydrazone formation in charged microdroplets. *Rapid Communications in Mass Spectrometry* **2016,** *30* (16), 1875-1878.
5. Wei, Z.; Li, Y.; Cooks, R. G.; Yan, X. Accelerated Reaction Kinetics in Microdroplets: Overview and Recent Developments. *Annual Review of Physical Chemistry* **2020,** *71* (Volume 71, 2020), 31-51.
6. Holden, D. T.; Morato, N. M.; Cooks, R. G. Aqueous microdroplets enable abiotic synthesis and chain extension of unique peptide isomers from free amino acids. *Proceedings of the National Academy of Sciences* **2022,** *119* (42), e2212642119.
7. Angle, K. J.; Crocker, D. R.; Simpson, R. M. C.; Mayer, K. J.; Garofalo, L. A.; Moore, A. N.; Mora Garcia, S. L.; Or, V. W.; Srinivasan, S.; Farhan, M.; Sauer, J. S.; Lee, C.; Pothier, M. A.; Farmer, D. K.; Martz, T. R.; Bertram, T. H.; Cappa, C. D.; Prather, K. A.; Grassian, V. H. Acidity across the interface from the ocean surface to sea spray aerosol. *Proceedings of the National Academy of Sciences* **2021,** *118* (2), e2018397118.
8. Buch, V.; Milet, A.; Vácha, R.; Jungwirth, P.; Devlin, J. P. Water surface is acidic. *Proceedings of the National Academy of Sciences* **2007,** *104* (18), 7342-7347.
9. Inokuchi, Y.; Nishi, N. Infrared Photodissociation Spectroscopy of Protonated Formic Acid and Acetic Acid Clusters. *The Journal of Physical Chemistry A* **2003,** *107* (51), 11319-11323.
10. Olesen, S. G.; Hammerum, S. Redshift or Adduct Stabilization—A Computational Study of Hydrogen Bonding in Adducts of Protonated Carboxylic Acids. *European Journal of Mass Spectrometry* **2009,** *15* (2), 239-248.
11. Sekiguchi, O.; Bakken, V.; Uggerud, E. Decomposition of protonated formic acid: One transition state - Two product channels. *J. Am. Soc. Mass Spectrom.* **2004,** *15* (7), 982-988.
12. Petrie, S.; Bohme, D. K. Ions in space. *Mass Spectrometry Reviews* **2007,** *26* (2), 258-280.
13. Klemperer, W. Astronomical Chemistry. *Annual Review of Physical Chemistry* **2011,** *62* (Volume 62, 2011), 173-184.
14. Mladenović, M.; Roueff, E. Ion-molecule reactions involving HCO+ and N2H+: Isotopologue equilibria from new theoretical calculations and consequences for interstellar isotope fractionation. *A&A* **2014,** *566*, A144.
15. Khuu, T.; Schleif, T.; Mohamed, A.; Mitra, S.; Johnson, M. A.; Valdiviezo, J.; Heindel, J. P.; Head-Gordon, T. Intra-cluster Charge Migration upon Hydration of Protonated Formic Acid Revealed by Anharmonic Analysis of Cold Ion Vibrational Spectra. *The Journal of Physical Chemistry A* **2023,** *127* (36), 7501-7509.
16. Wolk, A. B.; Leavitt, C. M.; Garand, E.; Johnson, M. A. Cryogenic Ion Chemistry and Spectroscopy. *Acc. Chem. Res.* **2014,** *47* (1), 202-210.
17. Wang, H.; Agmon, N. Complete Assignment of the Infrared Spectrum of the Gas-Phase Protonated Ammonia Dimer. *The Journal of Physical Chemistry A* **2016,** *120* (19), 3117-3135.
18. Thomas, M.; Brehm, M.; Fligg, R.; Vöhringer, P.; Kirchner, B. Computing vibrational spectra from ab initio molecular dynamics. *Physical chemistry chemical physics : PCCP* **2013,** *15* (18), 6608-6622.

19. Khuu, T.; Yang, N.; Johnson, M. A. Vibrational spectroscopy of the cryogenically cooled O- and N-protomers of 4-aminobenzoic acid: Tag effects, isotopic labels, and identification of the E,Z isomer of the O-protomer. *International Journal of Mass Spectrometry* **2020,** *457*, 116427.
20. Yang, N.; Duong, C. H.; Kelleher, P. J.; Johnson, M. A.; McCoy, A. B. Isolation of Site-Specific Anharmonicities of Individual Water Molecules in the $I^-\cdot(H_2O)_2$ Complex Using Tag-Free, Isotopomer Selective IR-IR Double Resonance. *Chem. Phys. Lett.* **2017,** *690*, 159-171.
21. Stropoli, S. J.; Greis, K.; Schleif, T.; Johnson, M. A. Characterization of Oxidation Products from HOCl Uptake by Microhydrated Methionine Anions Using Cryogenic Ion Vibrational Spectroscopy. *The Journal of Physical Chemistry A* **2023,** *127* (19), 4269-4276.
22. Khuu, T.; Rana, A.; Edington, S. C.; Yang, N.; McCoy, A. B.; Johnson, M. A. Observation of Slow Eigen-Zundel Interconversion in H+(H2O)6 Clusters upon Isomer-Selective Vibrational Excitation and Buffer Gas Cooling in a Cryogenic Ion Trap. *Journal of the American Society for Mass Spectrometry* **2023,** *34* (4), 737-744.
23. Harrilal, C. P.; DeBlase, A. F.; Fischer, J. L.; Lawler, J. T.; McLuckey, S. A.; Zwier, T. S. Infrared Population Transfer Spectroscopy of Cryo-Cooled Ions: Quantitative Tests of the Effects of Collisional Cooling on the Room Temperature Conformer Populations. *The Journal of Physical Chemistry A* **2018,** *122* (8), 2096-2107.
24. Duong, C. H.; Gorlova, O.; Yang, N.; Kelleher, P. J.; Johnson, M. A.; McCoy, A. B.; Yu, Q.; Bowman, J. M. Disentangling the Complex Vibrational Spectrum of the Protonated Water Trimer, H+(H2O)3, with Two-Color IR-IR Photodissociation of the Bare Ion and Anharmonic VSCF/VCI Theory. *The Journal of Physical Chemistry Letters* **2017,** *8* (16), 3782-3789.
25. Frisch, M. J.; Trucks, G. W.; Schlegel, H. B.; Scuseria, G. E.; Robb, M. A.; Cheeseman, J. R.; Scalmani, G.; Barone, V.; Petersson, G. A.; Nakatsuji, H.; Li, X.; Caricato, M.; Marenich, A. V.; Bloino, J.; Janesko, B. G.; Gomperts, R.; Mennucci, B.; Hratchian, H. P.; Ortiz, J. V.; Izmaylov, A. F.; Sonnenberg, J. L.; Williams; Ding, F.; Lipparini, F.; Egidi, F.; Goings, J.; Peng, B.; Petrone, A.; Henderson, T.; Ranasinghe, D.; Zakrzewski, V. G.; Gao, J.; Rega, N.; Zheng, G.; Liang, W.; Hada, M.; Ehara, M.; Toyota, K.; Fukuda, R.; Hasegawa, J.; Ishida, M.; Nakajima, T.; Honda, Y.; Kitao, O.; Nakai, H.; Vreven, T.; Throssell, K.; Montgomery Jr., J. A.; Peralta, J. E.; Ogliaro, F.; Bearpark, M. J.; Heyd, J. J.; Brothers, E. N.; Kudin, K. N.; Staroverov, V. N.; Keith, T. A.; Kobayashi, R.; Normand, J.; Raghavachari, K.; Rendell, A. P.; Burant, J. C.; Iyengar, S. S.; Tomasi, J.; Cossi, M.; Millam, J. M.; Klene, M.; Adamo, C.; Cammi, R.; Ochterski, J. W.; Martin, R. L.; Morokuma, K.; Farkas, O.; Foresman, J. B.; Fox, D. J. *Gaussian 16 Rev. C.01*, Wallingford, CT, 2016.
26. McCunn, L. R.; Roscioli, J. R.; Elliott, B. M.; Johnson, M. A.; McCoy, A. B. Why Does Argon Bind to Deuterium? Isotope Effects and Structures of $Ar\cdot H_5O_2^+$ Complexes. *J. Phys. Chem. A* **2008,** *112* (27), 6074-6078.
27. Dickenson, G. D.; Niu, M. L.; Salumbides, E. J.; Komasa, J.; Eikema, K. S. E.; Pachucki, K.; Ubachs, W. Fundamental Vibration of Molecular Hydrogen. *Physical Review Letters* **2013,** *110* (19), 193601.
28. Pettersson, M.; Lundell, J.; Khriachtchev, L.; Räsänen, M. IR Spectrum of the Other Rotamer of Formic Acid, cis-HCOOH. *J Am Chem Soc* **1997,** *119* (48), 11715-11716.
29. DeLuca, M. J.; Cyr, D. M.; Chupka, W. A.; Johnson, M. A. Isotopic fractionation in low temperature ion–molecule exchange reactions: Enrichment of 22Ne in Ne+n clusters formed by association in an ionized free jet. *The Journal of Chemical Physics* **1990,** *92* (12), 7349-7355.
30. DeVine, J. A.; Debnath, S.; Li, Y.-K.; McCaslin, L. M.; Schöllkopf, W.; Neumark, D. M.; Asmis, K. R. Infrared photodissociation spectroscopy of D2-tagged CH3CO2−(H2O)0−2 anions. *Mol Phys* **2020,** *118* (11), e1749953.
31. Roscioli, J. R.; McCunn, L. R.; Johnson, M. A. Quantum Structure of the Intermolecular Proton Bond. *Science* **2007,** *316*, 249-254.